

***SMAI-JCM***  
SMAI JOURNAL OF  
COMPUTATIONAL MATHEMATICS

A High-Order Integrator for the  
Schrödinger Equation with  
Time-Dependent, Homogeneous  
Magnetic Field

VASILE GRADINARU & OLIVER RIETMANN

Volume 6 (2020), p. 253-271.

<[http://smai-jcm.centre-mersenne.org/item?id=SMAI-JCM\\_2020\\_\\_6\\_\\_253\\_0](http://smai-jcm.centre-mersenne.org/item?id=SMAI-JCM_2020__6__253_0)>

© Société de Mathématiques Appliquées et Industrielles, 2020

*Certains droits réservés.*



*Publication membre du*

*Centre Mersenne pour l'édition scientifique ouverte*

<http://www.centre-mersenne.org/>

Sousmission sur <https://smai-jcm.math.cnrs.fr/index.php/SMAI-JCM>





# A High-Order Integrator for the Schrödinger Equation with Time-Dependent, Homogeneous Magnetic Field

VASILE GRADINARU <sup>1</sup>  
OLIVER RIETMANN <sup>2</sup>

<sup>1</sup> Seminar for Applied Mathematics, ETH Zurich, Switzerland  
*E-mail address:* vasile.gradinaru@math.ethz.ch

<sup>2</sup> Seminar for Applied Mathematics, ETH Zurich, Switzerland  
*E-mail address:* oliver.riemann@math.ethz.ch

**Abstract.** We construct a family of numerical methods for the Pauli equation of charged particles in a time-dependent, homogeneous magnetic field. These methods are described in a general setting comprising systems of multiple particles and extend the usual splitting and Fourier grid approach. The issue is that the magnetic field causes charged particles to rotate. The corresponding rotations of the wave function are highly incompatible with the Fourier grid approach used for the standard Schrödinger equation. Motivated by the theory of Lie algebras and their representations, our new approach approximates the exact flow map in terms of rotated potentials and rotated initial data, and thereby avoids this issue. Finally, we provide numerical examples to examine convergence and preservation of norm and energy.

**2020 Mathematics Subject Classification.** 81Q05, 65M12, 65M22.

**Keywords.** quantum mechanics, time-dependent Schrödinger equation, magnetic field, discrete Fourier transform, numerical method, splitting, convergence rate, Lie group, Lie algebra.

## Introduction

The Pauli equation as introduced in 1927 describes an electron in an external, homogeneous magnetic field [17]. Though formulated almost one century ago, it is still used in modern applications, e.g. ion traps used to realize qubits in quantum computing: the Penning trap confines charged particles in a homogeneous magnetic field and is modelled by the Pauli equation [20].

For the standard Schrödinger equation (i.e. zero magnetic field), splitting methods in combination with FFT have been used for instance in [1] and are standard by now. The presence of a magnetic field gives rise to a new term in the Hamiltonian, we call it the magnetic term. Several attempts have been made to adapt the standard splitting/FFT approach to the magnetic Schrödinger equation [14, 4, 11].

We provide a novel method to handle the magnetic term via splitting and FFT. The efficiency of our method is comparable to the standard one for zero magnetic field and also maintains the advantages of the latter, such as natural norm preservation and exponential convergence in space. The spectral approach which is the key to exponential convergence in space requires magnetic fields that depend only on time, but not on space. However, we allow for general potentials, depending on space and time.

Another spectral method that relies on splitting is presented in [22], where generalized coherent states (so called Hagedorn wavepackets) are used instead of the Fourier grid. This approach improves for small values of the model parameter in [7], while the Fourier grid approach is suited for large values.

### 1. The Mathematical Model

Consider a spinless<sup>1</sup> particle of mass  $m > 0$  and charge  $e \in \mathbb{R}$  living in  $\mathbb{R}^d$  subject to an electric potential  $\phi(x, t)$  and a magnetic potential 1-form  $A(x, t) = A_k(x, t)dx^k$ , where  $x \in \mathbb{R}^d$ . We assume the corresponding magnetic field 2-form  $dA$  to be independent of  $x$ . Therefore we choose

$$A(x, t) := \frac{1}{2}B_{jk}(t)x^j dx^k \tag{1.1}$$

where  $B(t) = (B_{jk}(t))_{1 \leq j, k \leq d}$  is a real, skew-symmetric matrix. The corresponding magnetic field 2-form is given by

$$dA = \sum_{1 \leq j < k \leq d} B_{jk}(t) dx^j \wedge dx^k.$$

We introduce for  $j, k \in \{1, \dots, d\}$  the operators [13, Eq (14)], [6, Eq (3.21)]

$$\begin{aligned} p_k &:= -i\hbar\partial_k && \text{(components of linear momentum)} \\ L_{jk} &:= x_j p_k - x_k p_j. && \text{(generalized angular momentum)} \end{aligned}$$

Our system is then described by the Pauli Hamiltonian

$$\begin{aligned} H_P(t) &:= \frac{1}{2m} \sum_{k=1}^d (p_k - eA_k(x, t))^2 + e\phi(x, t) \\ &= \frac{1}{2m} \left( \hbar^2(-\Delta) - e \sum_{1 \leq j < k \leq d} B_{jk}(t)L_{jk} + \frac{e^2}{4} \|B(t)x\|_{\mathbb{R}^d}^2 \right) + e\phi(x, t). \end{aligned} \tag{1.2}$$

Upon redefining  $t, x, B$  and introducing a more general potential  $V(x, t)$ , we may instead consider the new Hamiltonian

$$H(t) := -\Delta + H_B(t) + V(x, t) \tag{1.3}$$

on<sup>2</sup>  $L^2(\mathbb{R}^d)$ , where (now  $\hbar = 1$ )

$$\begin{aligned} p_k &= -i\partial_k \\ L_{jk} &= x_j p_k - x_k p_j \\ H_B(t) &:= - \sum_{1 \leq j < k \leq d} B_{jk}(t)L_{jk} \end{aligned} \tag{1.4}$$

with associated Schrödinger equation

$$i\partial_t \psi(x, t) = H(t)\psi(x, t), \quad \psi_0(x) = \psi(x, 0). \tag{H}$$

Note that this equation is more general as  $V(x, t)$  can also contain an external potential besides  $\phi(x, t)$ .

**Remark 1.1.** If we choose in (1.3)

$$V(x, t) = \|B(t)x\|_{\mathbb{R}^d}^2 + \phi(x, t),$$

we recover (up to scaling) the potential terms in the physical Pauli Hamiltonian (1.2).

The paper is organized as follows: Section 2 describes a numerical method for (H), where each subsection deals with one subproblem. Physical applications and concrete examples of the abstract setting above are in Section 3.

<sup>1</sup>Our theory can easily be extended to particles that carry spin. This is explained in Subsection 3.1.

<sup>2</sup>We write  $L^2(\mathbb{R}^d) := L^2(\mathbb{R}^d; \mathbb{C})$  for the **complex-valued**, square-integrable functions.

## 2. The Numerical Method

We split (H) into the three simpler equations:

$$i\partial_t\psi(x, t) = -\Delta\psi(x, t) \tag{K}$$

$$i\partial_t\psi(x, t) = H_B(t)\psi(x, t) \tag{M}$$

$$i\partial_t\psi(x, t) = V(x, t)\psi(x, t) \tag{P}$$

The main steps of our method are:

- (1) Solve the potential equation (P) using pointwise multiplication by  $e^{-i\int_{t_0}^t V(x,s)ds}$ .
- (2) Solve the kinetic equation (K) in the (discrete) Fourier space.
- (3) Reduce the magnetic equation (M) to the linear ODE<sup>3</sup>

$$\frac{d}{dt}y(t) = B(t)y(t), \tag{B}$$

where  $y : \mathbb{R} \rightarrow \mathbb{R}^d$ . This is achieved using a Lie algebra isomorphism relating  $B(t)$  and  $H_B(t)$ . We then use Magnus expansion to solve (B).

- (4) Using that  $-\Delta$  and  $H_B(t)$  commute, combine the previous solutions to a solution of

$$i\partial_t\psi = (-\Delta + H_B(t))\psi. \tag{K+M}$$

- (5) A splitting scheme merges the solutions from Steps 4 and 1 to a solution of (H).

Since Steps 1 and 2 are standard, we discuss only Steps 3, 4 and 5 in detail. Step 5 includes a fundamentally new idea which makes the algorithm applicable for any Fourier grid in space and time and hence feasible in higher dimensions. For convenience, we use exclusively uniform grids and standard FFT in our numerical experiments. Finally, we introduce the following notation: Given a Hamiltonian  $\tilde{H}(t)$  we denote by  $\Phi_{\tilde{H}}(t, t_0)$  the unitary flow associated with the time-dependent Schrödinger equation

$$i\partial_t\psi(x, t) = \tilde{H}(t)\psi(x, t), \quad \psi_0(x) = \psi(x, 0),$$

i.e.  $\Phi_{\tilde{H}}(t, t_0)$  satisfies

$$\frac{d}{dt}\Phi_{\tilde{H}}(t, t_0) = -i\tilde{H}(t)\Phi_{\tilde{H}}(t, t_0), \quad \Phi_{\tilde{H}}(t_0, t_0) = \text{id}. \tag{2.1}$$

### 2.1. Step 3: Solving Equation (M)

Let  $\text{SO}(d)$  denote the special orthogonal group of real  $d \times d$  matrices. Note that [18, Thm X.69] yields existence of a flow map  $U(t, t_0) \in \text{SO}(d)$  solving (B), i.e.

$$\frac{d}{dt}U(t, t_0) = B(t)U(t, t_0), \quad U(t_0, t_0) = \text{id}. \tag{2.2}$$

To accomplish a link between equations (B) and (M), we consider the group  $U(L^2(\mathbb{R}^d))$  of unitary operators on  $L^2(\mathbb{R}^d)$  and the unitary representation

$$\rho : \text{SO}(d) \longrightarrow U(L^2(\mathbb{R}^d))$$

defined as the map satisfying

$$(\rho(R)\psi)(x) = \psi(R^{-1}x) \tag{2.3}$$

for all  $R \in \text{SO}(d)$ ,  $\psi \in L^2(\mathbb{R}^d)$  and all  $x \in \mathbb{R}^d$ .

---

<sup>3</sup>After multiplication by  $i$  on both sides, (B) becomes a Schrödinger equation with Hamiltonian  $iB(t)$ .

**Lemma 2.1.** *The flow map  $U(t, t_0)$  of (B) gives rise to a flow map of (M) by*

$$\Phi_{H_B}(t, t_0) = \rho(U(t, t_0))$$

for all  $t, t_0 \in \mathbb{R}$ .

**Proof.** Observe that

$$-iH_B(t) = \sum_{j,k=1}^d B_{jk}(t)x_j\partial_k. \quad (2.4)$$

and fix  $t, t_0 \in \mathbb{R}$ . For all  $j, k \in \{1, \dots, d\}$  and all  $x \in \mathbb{R}^d$ , we have

$$x_j\partial_k\psi_0(U^{-1}(t, t_0)x) = d\psi_0|_{U^{-1}(t, t_0)x} \cdot x_j\partial_k U^{-1}(t, t_0)x = d\psi_0|_{U^{-1}(t, t_0)x} \cdot U^{-1}(t, t_0)x_j\partial_k x.$$

Hence by (2.4) and linearity

$$-iH_B(t)\psi_0(U^{-1}(t, t_0)x) = d\psi_0|_{U^{-1}(t, t_0)x} \cdot U^{-1}(t, t_0)(-iH_B(t)x).$$

Anti-symmetry of  $B(t)$  and (2.4) yield similarly for all  $x \in \mathbb{R}^d$

$$-iH_B(t)x = -B(t)x.$$

We take the transpose on both sides of (2.2) and use anti-symmetry of  $B(t)$  again in order to get

$$\frac{d}{dt}U^{-1}(t, t_0) = (-1)U^{-1}(t, t_0)B(t).$$

Fix some initial data  $\psi_0 \in L^2(\mathbb{R})$ . Using the last three equations, we compute

$$\begin{aligned} -iH_B(t)\psi_0(U^{-1}(t, t_0)x) &= d\psi_0|_{U^{-1}(t, t_0)x} \cdot U^{-1}(t, t_0)(-iH_B(t)x) \\ &= d\psi_0|_{U^{-1}(t, t_0)x} \cdot (-1)U^{-1}(t, t_0)B(t)x \\ &= d\psi_0|_{U^{-1}(t, t_0)x} \cdot \frac{d}{dt}U^{-1}(t, t_0)x \\ &= \frac{d}{dt}\psi_0(U^{-1}(t, t_0)x). \end{aligned}$$

Hence  $\rho(U(t, t_0))$  is a flow map for (M). ■

There is a more general principle behind the last lemma, which involves the theory of Lie groups, Lie algebras, and their representation theory. The rest of this subsection is rather technical and briefly explains this principle. But for our purpose, Lemma 2.1 will suffice. The reader may thus continue with Subsection 2.2 if he is only interested in the numerical method.

Besides the group structure,  $\mathrm{SO}(d)$  is a manifold, more precisely a Lie group. Its tangent space at the identity, endowed with the matrix commutator, is called the Lie algebra

$$\mathfrak{so}(d) := \{\Omega \in \mathbb{R}^{d \times d} \mid \Omega^T = -\Omega\}$$

of  $\mathrm{SO}(d)$ . Moreover, we consider the Lie algebra spanned by ( $i$  times) the angular momentum operators (1.4)

$$\mathfrak{l}(L^2(\mathbb{R}^d)) := \mathrm{span}_{\mathbb{R}}\{iL_{jk} \mid 1 \leq j < k \leq d\},$$

also endowed with the usual commutator<sup>4</sup>. The derivative of  $\rho$  is the Lie algebra isomorphism (compare [6, Eq (2.14)] and [6, Eq (3.28)])

$$\rho_* : \mathfrak{so}(d) \longrightarrow \mathfrak{l}(L^2(\mathbb{R}^d)), \quad \Omega \longmapsto -iH_{\Omega}.$$

---

<sup>4</sup>The notation  $\mathfrak{l}(L^2(\mathbb{R}^d))$  is **not** standard.

Note that  $B(t) \in \mathfrak{so}(d)$  for all  $t \in \mathbb{R}$ . We see that  $\rho$  maps the flow of (B) to the flow of (M) because  $\rho_*$  maps  $B(t)$  to  $-iH_B(t)$  (i.e. relates the right-hand-sides of the two equations). This relation is summarized in the following commuting diagram

$$\begin{array}{ccc} \mathfrak{so}(d) & \xrightarrow{\rho_*} & \mathfrak{l}(L^2(\mathbb{R}^d)) \\ \exp \downarrow & & \downarrow \exp \\ \mathrm{SO}(d) & \xrightarrow{\rho} & \mathrm{U}(L^2(\mathbb{R}^d)) \end{array}$$

where  $\exp$  denotes the exponential map from a tangent space into its manifold.

### 2.2. Step 3: Solving Equation (B) by Magnus Expansion

We approximate the exact flow  $U(t, t_0) \in \mathrm{SO}(d)$  of (B) by a Magnus expansion (see [15] or [10, Ch IV.7] for details), i.e.

$$U(t, t_0) \approx U_n(t, t_0) := e^{\Omega^{[n]}(t, t_0)}, \quad \Omega^{[n]}(t, t_0) := \sum_{m=1}^n \Omega_m(t, t_0), \quad (2.5)$$

for some  $\Omega_m(t, t_0) \in \mathfrak{so}(d)$  and the first two terms of the truncated series are

$$\Omega_1(t, t_0) = \int_{t_0}^t B(s_1) ds_1, \quad \Omega_2(t, t_0) = \frac{1}{2} \int_{t_0}^t \int_{t_0}^{s_1} [B(s_1), B(s_2)] ds_2 ds_1.$$

The Magnus expansion yields a unitary approximation of  $\Phi_{H_B}(t, t_0) = \rho(U(t, t_0))$  as stated in the next lemma.

**Lemma 2.2.** *For all  $t, t_0 \in \mathbb{R}$  and all  $n \in \mathbb{N}$ , we have*

- (i)  $U_n(t, t_0) \in \mathrm{SO}(d)$  and
- (ii)  $\rho(U_n(t, t_0))$  is a unitary map on  $L^2(\mathbb{R}^d)$ .

**Proof.** Part (i) holds since the matrix exponential on a Lie algebra maps to its Lie group. Moreover, (i) implies (ii) by means of the substitution  $y := U_n^{-1}(t, t_0)x$  in the integral of the inner product on  $L^2(\mathbb{R}^d)$ . ■

**Example 2.3.** In all subsequent simulations, we use the following fourth order commutator free Magnus integrator from Example 1 in [3]. Define the nodes and weights

$$c := \begin{pmatrix} \frac{1}{2} - \frac{\sqrt{3}}{6} \\ \frac{1}{2} + \frac{\sqrt{3}}{6} \end{pmatrix}, \quad \alpha := \begin{pmatrix} \frac{1}{4} - \frac{\sqrt{3}}{6} \\ \frac{1}{4} + \frac{\sqrt{3}}{6} \end{pmatrix}.$$

For a sufficiently small time step  $h > 0$  we define the orthogonal matrix

$$\tilde{U}(h, t_0) := \exp(\alpha_1 h B_1 + \alpha_2 h B_2) \cdot \exp(\alpha_2 h B_1 + \alpha_1 h B_2), \quad B_i := B(t_0 + c_i h).$$

For the uniform time grid  $t_j := t_0 + jh$ , where  $j \in \{0, \dots, J\}$  and  $t := t_J$ , we have

$$U(t, t_0) = \prod_{j=0}^J \tilde{U}(t_j, t_{j-1}) + O(h^5).$$

As pointed out in [3], the fourth order convergence is due to [1, Eq (12)].

**2.3. Step 4: Solving Equation (K+M)**

The following lemma shows that we can switch the flows and hence the internal steps in our algorithm in a convenient way. It also justifies the treatment of  $-\Delta$  and  $H_B$  together in one step.

**Lemma 2.4.** *Fix any  $t, t_0 \in \mathbb{R}$ . Then*

- (i) *for all  $R \in \text{SO}(d)$  the operators  $\rho(R)$  and  $\Phi_{-\Delta}(t, t_0)$  commute and*
- (ii) *we have  $\Phi_{-\Delta+H_B}(t, t_0) = \Phi_{H_B}(t, t_0) \Phi_{-\Delta}(t, t_0) = \Phi_{-\Delta}(t, t_0) \Phi_{H_B}(t, t_0)$ .*

**Proof.** Fix any  $R \in \text{SO}(d)$ . Note that  $\rho(R)$  commutes with the Fourier transform  $\mathcal{F}$  and that  $\mathbb{R}^d \rightarrow \mathbb{C}, k \mapsto e^{-i(t-t_0)k^2}$  is rotation invariant. Hence

$$\begin{aligned} \rho(R)e^{-i(t-t_0)(-\Delta)} &= \rho(R)\mathcal{F}^{-1}e^{-i(t-t_0)k^2}\mathcal{F} \\ &= \mathcal{F}^{-1}e^{-i(t-t_0)k^2}\mathcal{F}\rho(R) \\ &= e^{-i(t-t_0)(-\Delta)}\rho(R). \end{aligned}$$

This proves (i), which in turn proves the second equality in (ii) by Lemma 2.1. It remains to show that the first equality also holds:

$$\begin{aligned} \frac{d}{dt}(\Phi_{H_B}(t, t_0)\Phi_{-\Delta}(t, t_0)) &= \dot{\Phi}_{H_B}(t, t_0)\Phi_{-\Delta}(t, t_0) + \Phi_{H_B}(t, t_0)\dot{\Phi}_{-\Delta}(t, t_0) \\ &\stackrel{(2.1)}{=} -iH_B(t)\Phi_{H_B}(t, t_0)\Phi_{-\Delta}(t, t_0) - i\Phi_{H_B}(t, t_0)(-\Delta)\Phi_{-\Delta}(t, t_0) \\ &= -i(-\Delta + H_B(t))\Phi_{H_B}(t, t_0)\Phi_{-\Delta}(t, t_0), \end{aligned}$$

where we used rotation invariance of the Laplacian to swap  $-\Delta$  and  $\Phi_{H_B}(t, t_0)$ . It follows that  $\Phi_{H_B}(t, t_0)\Phi_{-\Delta}(t, t_0)$  solves (2.1) for  $\tilde{H} = -\Delta + H_B$ , which concludes the proof. ■

**2.4. Step 5: Solving Equation (H) by Splitting**

Let  $U(t, t_0)$  denote the flow map of (B) and  $\rho$  the left-regular representation defined in (2.3). We construct an approximation of the solution of the time-dependent Schrödinger Equation (H) associated with the full Hamiltonian

$$H(t) = -\Delta + H_B(t) + V(x, t)$$

by a splitting with coefficients<sup>5</sup>  $(a_i, b_i)_{i \in \{1, \dots, n\}}$ . We start with a few notations. Fix times  $t_0 < t$  and introduce for  $i \in \{0, \dots, n\}$  the time grids

$$t_i = t_0 + (t - t_0) \sum_{j=1}^i b_j \quad \text{and} \quad s_i = t_0 + (t - t_0) \sum_{j=1}^i a_j \tag{2.6}$$

and for any two Hamiltonians  $H_1$  and  $H_2$  write<sup>6</sup>

$$(\Phi_{H_2} \overset{(a,b)}{\circ} \Phi_{H_1})(t, t_0) := \prod_{i=0}^{n-1} \Phi_{H_2}(t_{i+1}, t_i)\Phi_{H_1}(s_{i+1}, s_i).$$

Our splitting scheme for (H) then reads

$$\Phi_H(t, t_0) \approx (\Phi_{-\Delta+H_B} \overset{(a,b)}{\circ} \Phi_V)(t, t_0) = \prod_{i=0}^{n-1} \Phi_{-\Delta}(t_{i+1}, t_i)\Phi_{H_B}(t_{i+1}, t_i)\Phi_V(s_{i+1}, s_i)$$

<sup>5</sup>For example we obtain the Strang splitting by  $a = (\frac{1}{2}, \frac{1}{2})$  and  $b = (1, 0)$ .

<sup>6</sup>The order of the product is “lowest index first”:  $\prod_{i=1}^n A_i := A_n \cdots A_1$

where we used part (ii) of Lemma 2.4. The equality

$$\rho(R)(f \cdot \psi) = (\rho(R)f) \cdot (\rho(R)\psi)$$

holds for all<sup>7</sup>  $\psi \in L^2(\mathbb{R}^d)$ ,  $f \in L^\infty(\mathbb{R}^d)$  and all  $R \in \text{SO}(d)$ . We apply it to the special choice  $R = U(t, t')$  and  $f(x) = e^{-i \int_{s'}^s V(x, \bar{s}) d\bar{s}}$ . Lemma 2.1 yields then

$$\Phi_{H_B}(t, t') \Phi_V(s, s') = \Phi_{\rho(U(t, t'))V}(s, s') \Phi_{H_B}(t, t') \quad (2.7)$$

for all  $t, t', s, s' \in \mathbb{R}$ . This is crucial for proving Lemma 2.5 below, which provides an expression for  $(\Phi_{-\Delta+H_B} \overset{(a,b)}{\circ} \Phi_V)(t, t_0)$  in terms of rotated potentials and a single rotation of the initial data.

**Lemma 2.5.** *For splitting coefficients  $(a_i, b_i)_{i \in \{1, \dots, n\}}$  and times  $s_0, \dots, s_n, t_0, \dots, t_n, t$  as in (2.6), we have*

$$(\Phi_{-\Delta+H_B} \overset{(a,b)}{\circ} \Phi_V)(t, t_0) = \left( \prod_{i=0}^{n-1} \Phi_{-\Delta}(t_{i+1}, t_i) \Phi_{\rho(U(t_n, t_i))V}(s_{i+1}, s_i) \right) \Phi_{H_B}(t_n, t_0).$$

**Proof.** We proceed by induction on  $n$ . For  $n = 1$ , the assertion follows immediately from (2.7). Suppose now that the formula holds for any set of coefficients of length  $n - 1$ . Using this hypothesis on the last  $n - 1$  factors and Lemma 2.4, we obtain

$$\begin{aligned} (\Phi_{-\Delta+H_B} \overset{(a,b)}{\circ} \Phi_V)(t, t_0) &= \left( \prod_{i=1}^{n-1} \Phi_{-\Delta}(t_{i+1}, t_i) \Phi_{\rho(U(t_n, t_i))V}(s_{i+1}, s_i) \right) \Phi_{H_B}(t_n, t_1) \\ &\quad \times \Phi_{-\Delta}(t_1, t_0) \Phi_{H_B}(t_1, t_0) \Phi_V(s_1, s_0) \\ &= \left( \prod_{i=1}^{n-1} \Phi_{-\Delta}(t_{i+1}, t_i) \Phi_{\rho(U(t_{i+1}, t_i))V}(s_{i+1}, s_i) \right) \\ &\quad \times \Phi_{-\Delta}(t_1, t_0) \Phi_{H_B}(t_n, t_0) \Phi_V(s_1, s_0) \\ &= \left( \prod_{i=1}^{n-1} \Phi_{-\Delta}(t_{i+1}, t_i) \Phi_{\rho(U(t_n, t_i))V}(s_{i+1}, s_i) \right) \\ &\quad \times \Phi_{-\Delta}(t_1, t_0) \Phi_{\rho(U(t_n, t_0))V}(s_1, s_0) \Phi_{H_B}(t_n, t_0) \end{aligned}$$

which is exactly the claim for  $n$  factors. ■

## 2.5. The Main Result

The application of  $\Phi_{H_B}$  requires rotation of functions in their argument. This is impossible if the functions are defined on a grid as in the Fourier grid approach used for  $\Phi_{-\Delta}$ . However, we can rotate the initial data  $\psi_0(x)$  and the potential  $V(x, t)$  if they are given as concrete expressions. This is done by Equation (2.8) below, our main result. It provides an approximation of the flow map of (H) in terms of rotated potentials and a single rotation of the initial data. It uses only the flow maps  $\Phi_{-\Delta}$ ,  $\Phi_{H_B}$ ,  $\Phi_V$  which were discussed above.

In Lemma 2.5 we have only treated a single timestep  $[t_0, t]$ . If we generalize the idea to  $N$  steps of length  $h := t - t_0$ , we arrive at the following formula: For splitting coefficients  $(a_i, b_i)_{i \in \{1, \dots, n\}}$  and

<sup>7</sup>Even if  $f \notin L^2(\mathbb{R}^d)$  we still define  $\rho(R)f$  as in (2.3).

times  $s_0, \dots, s_n, t_0, \dots, t_n$  as in (2.6), we have

$$\begin{aligned} & \Phi_H(t_0 + Nh, t_0) \\ &= \left( \prod_{j=0}^{N-1} \prod_{i=0}^{n-1} \Phi_{-\Delta}(t_{i+1}, t_i) \Phi_{\rho(U(t_0+Nh, t_i+jh))V}(s_{i+1} + jh, s_i + jh) \right) \Phi_{H_B}(t_0 + Nh, t_0) + \mathcal{O}(h^p), \end{aligned} \quad (2.8)$$

for  $h \rightarrow 0$  and  $p \in \mathbb{N}$  is the order of the splitting scheme (see Table 2.1). Here we assume that  $U(t, t_0) \in \text{SO}(d)$  is the exact flow map defined in Equation (2.2). The right-hand side of (2.8) is an  $N$ -fold concatenation of

$$(\Phi_{-\Delta+H_B} \overset{(a,b)}{\circ} \Phi_V)(t, t_0),$$

followed by subsequent applications of (2.7). Since we can represent each of the involved propagators exactly, we expect the order of our method to be the order of the splitting scheme. However, we only provide a proof of consistency and convergence in the simplest case of the Lie-Trotter splitting ( $n = a_1 = b_1 = 1$ ) in Theorem 2.9 below. For higher order splittings we refer to the numerical experiments in Section 3, see Table 2.1 for a complete list of splitting methods used in these experiments. Algorithm 1 provides a pseudo-code for efficient computing of the right-hand side of (2.8).

TABLE 2.1. Several splitting methods. The first row provides labels for the legends of the plots in Section 3.

Method	Order $p$	Author(s)	Reference(s)
SS	2	Strang	[19], [9]: Page 42, Eq. 5.3
PRKS6	4	Blanes/Moan	[2]: Page 318, Table 2, ‘S6’
BM42	4	Blanes/Moan	[2]: Page 318, Table 3, ‘SRKNb6’
Y61	6	Yoshida	[21], [9]: Page 144, Eq. 3.11
KL6	6	Kahan/Li	[12], [9]: Page 144, Eq. 3.12
KL8	8	Kahan/Li	[12], [9]: Page 145, Eq. 3.14

**Remark 2.6.** It only remains to approximate the flow  $U(t, t_0)$ , for instance by a Magnus expansion as discussed in Example 2.3. Since this problem is low-dimensional, we can approximate  $U(t, t_0)$  up to machine precision by brute force in every timestep. Thus the order of convergence in (2.8) remains valid if we replace  $U(t, t_0)$  by its approximation. In the simulations in Section 3, we implement this as follows: We divide the time interval into  $\tilde{N} = \lceil 1001 \cdot (t - t_0) \rceil$  equidistant sub-intervals. Then we apply the Magnus expansion to each sub-interval und multiply the resulting rotation matrices. Since the Magnus expansion happens in a low-dimensional setting, the impact on the overall runtime is neglectable. The choice of  $\tilde{N}$  is tuned for the particular examples we consider. Other examples might require different tuning.

**Remark 2.7.** If for all  $t \in \mathbb{R}$  the potential  $V(x, t)$  is spherically symmetric, i.e.

$$\forall R \in \text{SO}(d) : \rho(R)V(x, t) = V(x, t),$$

then we may replace  $\rho(U(t_0 + Nh, t_i + jh))V = V$  in (2.8).

In [5], the authors give a general consistency and convergence result, stating that the classical order of consistency and convergence of splitting schemes carries over to the setting of time-independent, unbounded operators. We conjecture that the same ideas as in [5] can be used for splittings of time-dependent unbounded operators. However, for the sake of simplicity, we restrict ourselves to the simplest

---

**Algorithm 1** Compute the RHS of (2.8)
 

---

**Input:** first time step  $[t_0, t]$ ; number of time steps  $N$ ; meshgrid  $X$ ; initial wave function  $\psi_0$  at time  $t_0$ ; potential  $V$ ; splitting coefficients  $(a_i, b_i)_{i \in \{1, \dots, n\}}$ ; flow maps  $\Phi_{-\Delta}, \Phi_V$  and  $U$  corresponding to (K),(P) and (B);

**Output:**  $Y$  is the solution at time  $(t - t_0) \cdot N + t_0$  evaluated on  $X$ ;

```

1:  $h := t - t_0$ 
2:  $t_a := t_0$ 
3:  $t_b := t_0$ 
4:  $R := U(t_0 + N \cdot h, t_0)$ 
5:  $Y := \psi_0 \circ R^{-1}(X)$   $\{= (\rho(R)\psi_0)(X)\}$ 
6: for  $j = 0$  to  $N - 1$  do
7:   for  $i = 1$  to  $n$  do
8:      $\tilde{V} := V \circ R^{-1}$   $\{= \rho(R)V\}$ 
9:      $Y = \Phi_{\tilde{V}}(t_a + a_i \cdot h, t_a)Y$ 
10:     $R = R \cdot U^{-1}(t_b + b_i \cdot h, t_b)$ 
11:     $Y = \Phi_{-\Delta}(t_b + b_i \cdot h, t_b)Y$ 
12:     $t_a = t_a + a_i \cdot h$ 
13:     $t_b = t_b + b_i \cdot h$ 
14:   end for
15: end for
16: return  $Y$ 
    
```

---

possible case of the Lie-Trotter splitting ( $n = a_1 = b_1 = 1$ ), which contains already the basic ideas. Note that this was already done in a similar context in [4]. Moreover, we consider *only formal computations* to avoid the technicalities arising in the context of unbounded operators. To this end, we treat time-dependent operators, say  $\mathcal{C}(t)$ , such that  $i\mathcal{C}(t)$  is self-adjoint for all times. We denote the corresponding unitary propagator by  $\Phi_{\mathcal{C}}(t, t_0)$ , meaning that formally

$$\frac{d}{dt}\Phi_{\mathcal{C}}(t, t_0) = \mathcal{C}(t)\Phi_{\mathcal{C}}(t, t_0), \quad \Phi_{\mathcal{C}}(t_0, t_0) = \text{id}.$$

We denote its formal derivative by  $\dot{\mathcal{C}}(t)$ . If for example  $\mathcal{C}(t) = i\Delta - iH_B(t)$ , we have  $\dot{\mathcal{C}}(t) = -iH_{\partial_t B}(t)$ , where  $\partial_t B(t)$  is the magnetic field matrix differentiated in every entry. Likewise, if  $\mathcal{C}(t) = -iV(x, t)$ , we have  $\dot{\mathcal{C}}(t) = -i\partial_t V(x, t)$ . The next theorem provides a *formal* consistency and convergence result. The proof is analog to the one of [5, Thm 2].

**Theorem 2.8.** *Let  $i\mathcal{A}(t)$  and  $i\mathcal{B}(t)$  be two time-dependent, self-adjoint operators on a Hilbert space  $\mathcal{H}$ . Fix  $t, t_0 \in \mathbb{R}$  and let  $\Phi(t, t_0) = \Phi_{\mathcal{B}}(t, t_0)\Phi_{\mathcal{A}}(t, t_0)$  denote the Lie-Trotter splitting operator. Then for all  $\phi \in \mathcal{H}$ , we have*

$$\|\Phi(t, t_0)\phi - \Phi_{\mathcal{A}+\mathcal{B}}(t, t_0)\phi\| \leq (c_1(t_0, t, \mathcal{A}, \mathcal{B}, \phi) + c_2(t_0, t, \mathcal{A}, \mathcal{B}, \phi)) |t - t_0|^2$$

provided that the following constants exist

$$c_1(t_0, t, \mathcal{A}, \mathcal{B}, \phi) = \max_{t_0 \leq s, \tilde{s} \leq t} \|[\Phi_{\mathcal{B}}(s, t_0), \dot{\mathcal{A}}(s)] \Phi_{\mathcal{A}}(\tilde{s}, t_0)\phi\|$$

$$c_2(t_0, t, \mathcal{A}, \mathcal{B}, \phi) = \max_{t_0 \leq s, \tilde{s} \leq t} \|[\mathcal{B}(s), \mathcal{A}(s)] \Phi_{\mathcal{B}}(s, t_0)\Phi_{\mathcal{A}}(\tilde{s}, t_0)\phi\|.$$

Now let  $\varphi_N$  denote the approximate solution of the Lie-Trotter splitting after  $N \in \mathbb{N}$  timesteps up to a final time  $T = N(t - t_0) + t_0$ , applied to initial data  $\varphi(t_0) \in \mathcal{H}$ , where  $\varphi$  denotes the exact solution.

Then

$$\|\varphi_N - \varphi(T)\| \leq \max_{t_0 \leq s_0 \leq T} (c_1(s_0, T, \mathcal{A}, \mathcal{B}, \varphi(s_0)) + c_2(s_0, T, \mathcal{A}, \mathcal{B}, \varphi(s_0))) |t - t_0|,$$

provided that the maximum exists.

**Proof.** We compute the formal derivative of the splitting operator

$$\frac{d}{dt} \Phi(t, t_0) = (\mathcal{A}(t) + \mathcal{B}(t)) \Phi(t, t_0) + R(t, t_0),$$

where

$$R(t, t_0) = [\Phi_{\mathcal{B}}(t, t_0), \mathcal{A}(t)] \Phi_{\mathcal{A}}(t, t_0).$$

Thus the defect operator  $L(t, t_0) := \Phi(t, t_0) - \Phi_{\mathcal{A}+\mathcal{B}}(t, t_0)$  satisfies the initial value problem

$$\frac{d}{dt} L(t, t_0) = (\mathcal{A}(t) + \mathcal{B}(t)) L(t, t_0) + R(t, t_0), \quad L(t_0, t_0) = 0.$$

The variation-of-constants formula thus yields the integral expression

$$L(t, t_0) = \int_{t_0}^t \Phi_{\mathcal{A}+\mathcal{B}}(t, s) R(s, t_0) ds.$$

We decompose  $R(s, t_0) = r(s, t_0) \Phi_{\mathcal{A}}(s, t_0)$  with  $r(s, t_0) = [\Phi_{\mathcal{B}}(s, t_0), \mathcal{A}(s)]$ . We construct an integral expression for  $r(s, t_0)$  in the same way we did before for  $L(t, t_0)$ . Observe that  $r(s, t_0)$  solves the initial values problem

$$\frac{d}{ds} r(s, t_0) = \mathcal{B}(s) r(s, t_0) + \tilde{R}(s, t_0), \quad r(t_0, t_0) = 0,$$

where

$$\tilde{R}(s, t_0) = [\Phi_{\mathcal{B}}(s, t_0), \dot{\mathcal{A}}(s)] + [\mathcal{B}(s), \mathcal{A}(s)] \Phi_{\mathcal{B}}(s, t_0).$$

As before, the variation-of-constants formula thus yields the integral expression

$$r(s, t_0) = \int_{t_0}^s \Phi_{\mathcal{B}}(s, \tilde{s}) \tilde{R}(\tilde{s}, t_0) d\tilde{s}.$$

If we insert this into the integral expression for  $L(t, t_0)$ , we obtain

$$L(t, t_0) = \int_{t_0}^t \Phi_{\mathcal{A}+\mathcal{B}}(t, s) \left( \int_{t_0}^s \Phi_{\mathcal{B}}(s, \tilde{s}) \tilde{R}(\tilde{s}, t_0) d\tilde{s} \right) \Phi_{\mathcal{A}}(s, t_0) ds.$$

Hence for all  $\phi \in \mathcal{H}$ , we have

$$\begin{aligned} \|L(t, t_0)\phi\| \leq & \left( \max_{t_0 \leq s, \tilde{s} \leq t} \|[\Phi_{\mathcal{B}}(s, t_0), \dot{\mathcal{A}}(s)] \Phi_{\mathcal{A}}(\tilde{s}, t_0)\phi\| \right. \\ & \left. + \max_{t_0 \leq s, \tilde{s} \leq t} \|[\mathcal{B}(s), \mathcal{A}(s)] \Phi_{\mathcal{B}}(s, t_0) \Phi_{\mathcal{A}}(\tilde{s}, t_0)\phi\| \right) |t - t_0|^2. \end{aligned}$$

This implies the local error formula in the claim. The global error follows by a standard Lady Windermere's Fan argument (see [5, Eq (5.6)] and [8, Fig 7.1]). ■

The idea is that a rapidly decaying and smooth initial data compensates for a growing but smooth potential  $V(x, t)$ , so that the constants  $c_1$  and  $c_2$  in Theorem 2.8 can be uniformly bounded on a compact time interval. Then we can infer local and global convergence of order 1 in case of the Lie-Trotter splitting. But instead of searching for minimal requirements in our context, we will just make this part of our assumptions.

**Theorem 2.9.** *Let  $U(t, t_0) \in \text{SO}(d)$  be the exact flow map defined in Equation (2.2). Suppose that the constants  $c_1$  and  $c_2$  in Theorem 2.8 exist and are finite on the interval  $[t_0, T]$  when applied to  $i\mathcal{A}(t) = V(x, t)$  and  $i\mathcal{B}(t) = -\Delta + H_B(t)$ . Then, in the case of the Lie-Trotter splitting ( $n = a_1 = b_1 = 1$ ), the method (2.8) is of consistency and convergence order 1.*

**Proof.** The right-hand side of (2.8) is an  $N$ -fold concatenation of Lemma 2.5, followed by subsequent applications of (2.7). Hence the order of convergence is equal to the one of the single step method in Lemma 2.5, i.e. of

$$(\Phi_{-\Delta+H_B} \circ \Phi_V)(t, t_0).$$

Recall that  $\Phi_{-\Delta+H_B} = \Phi_{-\Delta} \circ \Phi_{H_B}$  by Lemma 2.4. Since we can represent all three flow maps  $\Phi_{-\Delta}, \Phi_{H_B}, \Phi_V$  exactly, Theorem 2.8 finishes the proof.  $\blacksquare$

### 3. Examples

The Pauli Hamiltonian (1.2) (and thus also its abstract version (1.3)) contains many physically relevant cases. In order to investigate them, it is convenient to introduce the notation

$$\Omega(\vec{B}) := \begin{pmatrix} 0 & -B_3 & B_2 \\ B_3 & 0 & -B_1 \\ -B_2 & B_1 & 0 \end{pmatrix}, \quad \vec{B} = \begin{pmatrix} B_1 \\ B_2 \\ B_3 \end{pmatrix} \in \mathbb{R}^3.$$

**Example 3.1** ( $N$  particles in three dimensions). Consider a system of  $N$  particles of mass  $m > 0$  and charge  $e \in \mathbb{R}$  where  $n \in \{1, \dots, N\}$ , subject to an electric potential  $\phi(\vec{x}_1, \dots, \vec{x}_N, t)$  and a homogeneous magnetic field  $\vec{B}(t)$ . This system is modeled by the Pauli Hamiltonian

$$H_N = \frac{1}{2m} \sum_{n=1}^N \left( \vec{p}_n - e\vec{A}(\vec{x}_n, t) \right)^2 + e\phi(\vec{x}_1, \dots, \vec{x}_N, t)$$

where  $\vec{p}_n := -i\hbar\vec{\nabla}_n$  and the vector potential is given by

$$\vec{A}(\vec{x}, t) := \frac{1}{2}\vec{B}(t) \times \vec{x}.$$

By choosing  $d = 3N$  and

$$B(t) = \text{diag}(\Omega(-\vec{B}(t)), \dots, \Omega(-\vec{B}(t)))$$

in (1.1) we can obtain this as special case of (1.2).

**Example 3.2** ( $N$  particles in two dimensions). The setting of Example 3.1 can be adapted to  $N$  particles moving only in the  $(x, y)$ -plane. The magnetic field can be assumed perpendicular to the plane of motion, say  $\vec{B}(t) = (0, 0, B_3(t))^T$ . Thus we have to choose  $d = 2N$  and

$$B(t) = \text{diag} \left( \begin{pmatrix} 0 & B_3 \\ -B_3 & 0 \end{pmatrix}, \dots, \begin{pmatrix} 0 & B_3 \\ -B_3 & 0 \end{pmatrix} \right)$$

in (1.1) to retrieve this system as a special case of (1.2).

**Remark 3.3.** By Remark 1.1, we can recover (1.2) (up to scaling) from (1.3) by choosing

$$V(x, t) = \|B(t)x\|_{\mathbb{R}^d}^2 + \phi(x, t).$$

The integral of the magnetic part in the associated unitary flow

$$\Phi_V(t, t_0) = \exp \left( -i \int_{t_0}^t V(x, s) ds \right)$$

can be computed independently of  $x \in \mathbb{R}^d$  (and thus efficiently) since

$$\begin{aligned} \int_{t_0}^t V(x, s) ds &= \int_{t_0}^t \langle B(s)x, B(s)x \rangle_{\mathbb{R}^d} ds + \int_{t_0}^t \phi(x, s) ds \\ &= \left\langle x, \left( - \int_{t_0}^t B^2(s) ds \right) x \right\rangle_{\mathbb{R}^d} + \int_{t_0}^t \phi(x, s) ds \end{aligned}$$

where we used the skew-symmetry of  $B$  in the last step. For the integral of the electric potential part, we require an analytical expression, as computing an integral at every point  $x \in \mathbb{R}^d$  is expensive.

**Remark 3.4.** The assumption that all particles share the same mass and charge is only for simplicity. Redefining the coordinates  $x, t$  as well as  $B$  and  $V$  allows us to reduce the general case to one of the examples above.

**Remark 3.5.** Note that the block form of  $B(t)$  in the previous examples simplifies the computation of the exponential in the Magnus expansion (2.5): In the notation of (2.5), the matrices  $\Omega_m(t, t_0)$  inherit the block form. Similarly,  $\Omega^{[n]}(t, t_0)$  and  $U_n(t, t_0) = e^{\Omega^{[n]}(t, t_0)}$  become block-diagonal.

### 3.1. Spin

We have only treated spinless particles so far. However, in case of a single particle in a time-dependent, but homogeneous (in space) magnetic field, this is not a restriction. To see this, we consider a single particle ( $N = 1$ ) of spin  $\frac{1}{2}$ . We obtain the corresponding Hamiltonian if we extend  $H_1$  of Example 3.1 by the Stern-Gerlach term,

$$H_1^{\frac{1}{2}} = \begin{pmatrix} H_1 & 0 \\ 0 & H_1 \end{pmatrix} - \frac{e\hbar}{2m} \vec{\sigma} \cdot \vec{B}(t),$$

where we have introduced the Pauli matrices

$$\sigma_1 = \begin{pmatrix} 0 & 1 \\ 1 & 0 \end{pmatrix}, \quad \sigma_2 = \begin{pmatrix} 0 & -i \\ i & 0 \end{pmatrix}, \quad \sigma_3 = \begin{pmatrix} 1 & 0 \\ 0 & -1 \end{pmatrix}, \quad \vec{\sigma} = \begin{pmatrix} \sigma_1 \\ \sigma_2 \\ \sigma_3 \end{pmatrix}$$

and  $H_1^{\frac{1}{2}}$  acts on the two-component wave function

$$\psi(\vec{x}, t) = \begin{pmatrix} \psi_+(\vec{x}, t) \\ \psi_-(\vec{x}, t) \end{pmatrix}.$$

We provide an expression for the time evolution of  $H_1^{\frac{1}{2}}$ , in terms of the evolution operators for  $H_1$  and for the Schrödinger equation of the Stern-Gerlach term

$$i\partial_t \psi(\vec{x}, t) = -\frac{e\hbar}{2m} \vec{\sigma} \cdot \vec{B}(t) \psi(\vec{x}, t). \tag{S}$$

We apply the same reasoning to Equation (S) as for Equation (M): By [18, Thm. X.69], the evolution operator of (S) is given by some  $U(t, t_0) \in \text{SU}(2)$ , independent of  $\vec{x}$ . Here, we use that  $\vec{B}$  is independent of  $\vec{x}$ . Moreover, since  $U(t, t_0)$  is independent of  $\vec{x}$ , it commutes with the time evolution  $\Phi_{H_1}(t, t_0)$  of  $H_1$ . Thus, the time evolution of  $H_1^{\frac{1}{2}}$  reads

$$\Phi_{H_1^{\frac{1}{2}}}(t, t_0) = \begin{pmatrix} \Phi_{H_1}(t, t_0) & 0 \\ 0 & \Phi_{H_1}(t, t_0) \end{pmatrix} \cdot U(t, t_0) = U(t, t_0) \cdot \begin{pmatrix} \Phi_{H_1}(t, t_0) & 0 \\ 0 & \Phi_{H_1}(t, t_0) \end{pmatrix}.$$

One can approximate  $U(t, t_0)$  by a Magnus expansion as explained in Subsection 2.2. The time evolution of  $H_1$ , i.e. the spinless case, was discussed in detail above.

### 3.2. Order of Convergence (Harmonic Potential)

We now examine the order of convergence of our method for different splittings (see step 5). Therefore, we solve (H) for  $t \in [0, 2\pi]$  with magnetic field

$$B(t) = \Omega(-\vec{B}(t)), \quad \vec{B}(t) = \frac{\cos(t)}{\sqrt{3}} \begin{pmatrix} 1 \\ 1 \\ 1 \end{pmatrix}.$$

The potential in (1.3) is chosen as<sup>8</sup>

$$V(\vec{x}, t) = x_1^2 + x_2^2 + x_3^2.$$

The initial data at time  $t_0 = 0$  shall be the Gaussian

$$\psi_0(\vec{x}) = \frac{1}{(2\pi\sigma^2)^{\frac{3}{4}}} \exp\left(-\frac{(\vec{x} - \vec{\mu})^2}{4\sigma^2} + 2ix_1\right), \quad \vec{\mu} := \begin{pmatrix} 1 \\ 1 \\ 1 \end{pmatrix}, \quad \sigma^2 := \frac{1}{2} \quad (3.1)$$

of  $L^2$ -norm one. This setting admits periodic solutions of period  $2\pi$ . In particular, the solution  $\psi(\vec{x}, t)$  to this IVP satisfies  $\psi_0(\vec{x}) = \psi(\vec{x}, 2\pi)$  for all  $\vec{x} \in \mathbb{R}^3$ . The initial data will thus serve as reference solution for the convergence plots in Figure 3.1. They indicate that the order of our method is equal to the order of the underlying splitting scheme. In particular, it is not limited by the order 4 of the Magnus expansion, see Remark 2.6 for an explanation. We use a dense Fourier grid of equidistant meshwidth  $8\pi \cdot 2^{-7}$  in each spacial direction filling the cube  $[-4\pi, 4\pi]^3$ .

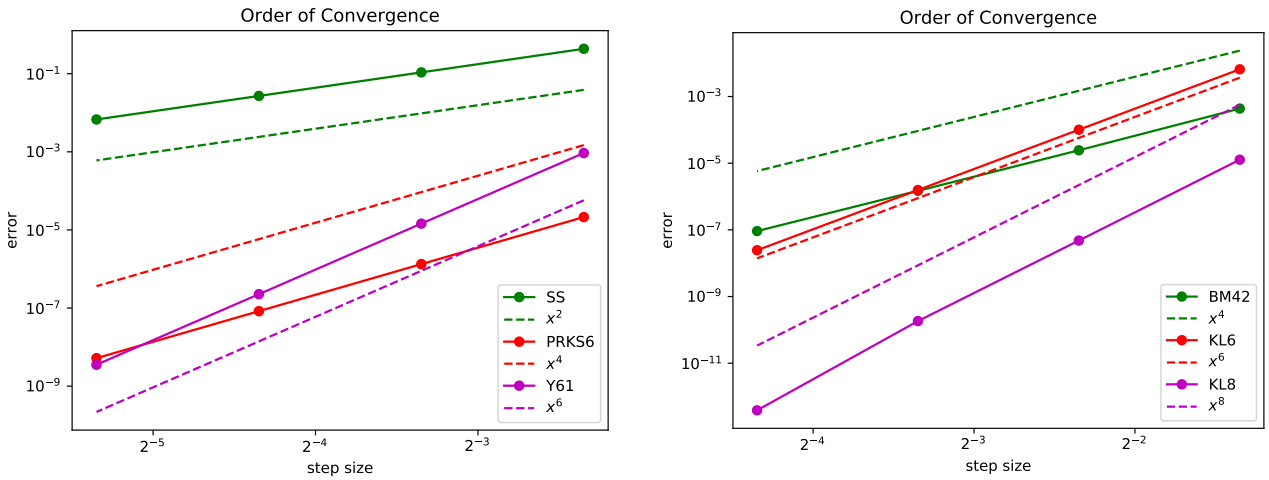


FIGURE 3.1. Order of convergence using different splittings. See Table 2.1 for the legend.

### 3.3. Order of Convergence (Mexican Hat Potential)

Now we consider the more involved example of a Mexican hat potential

$$\phi(\vec{x}) = \frac{1}{32} \|\vec{x}\|_{\mathbb{R}^3}^4 - x_1^2 - \frac{3}{2}x_2^2 - 2x_3^2.$$

<sup>8</sup>This is *not* a special case of the Pauli Hamiltonian (1.2) since  $V(\vec{x}, t)$  is independent of the magnetic field. Compare to Remark 1.1.

The magnetic field is given by

$$B(t) = \Omega(-\vec{B}(t)), \quad \vec{B}(t) = \frac{1}{\sqrt{3}} \begin{pmatrix} \cos(t) \\ \sin(t) \\ 1 \end{pmatrix}.$$

Thus we arrive at the time-dependent potential (see Remark 1.1)

$$V(\vec{x}, t) = \|B(t)\vec{x}\|_{\mathbb{R}^3}^2 + \phi(\vec{x}).$$

We solve the corresponding time-dependent Schrödinger equation (H) on  $t \in [0, 2\pi]$  using different splitting schemes. As before, (3.1) serves as initial data. The accurate KL8 splitting with time steps of size  $h = 2\pi \cdot 2^{-8}$  provides the reference solution for the results in Figure 3.2. The order of convergence is not limited by the order 4 of the Magnus expansion, see Remark 2.6 for an explanation. We use a dense Fourier grid of equidistant meshwidth  $8\pi \cdot 2^{-7}$  in each spacial direction filling the cube  $[-4\pi, 4\pi]^3$ .

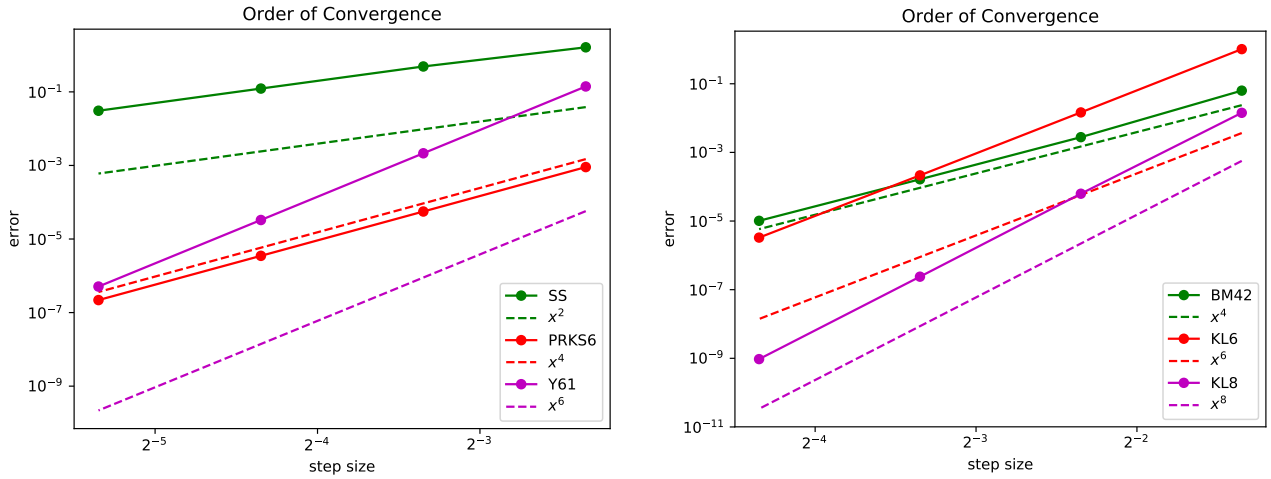


FIGURE 3.2. Order of convergence using different splittings. See Table 2.1 for the legend.

### 3.4. Norm and Energy Conservation (Morse Potential)

In this example we focus on the conservation of the  $L^2$ -norm and of the energy. The latter is conserved if the Hamiltonian is constant in time. We thus consider a modification of the Example 3.2 to the threefold Morse potential (see Figure 3.3)

$$\phi(x) = 16 \left( 1 - \exp \left( - \frac{\|x\|_{\mathbb{R}^2}^2}{32} (1 - \cos(3 \arctan 2(x_2, x_1)))^2 \right) \right)^2$$

and the constant magnetic field

$$B(t) = \frac{1}{2} \begin{pmatrix} 0 & -1 \\ 1 & 0 \end{pmatrix}$$

perpendicular to the plane of motion. The overall potential is hence now time-independent (see Remark 1.1)

$$V(x, t) = \|B(t)x\|_{\mathbb{R}^2}^2 + \phi(x) = \frac{1}{4} \|x\|_{\mathbb{R}^2}^2 + \phi(x)$$

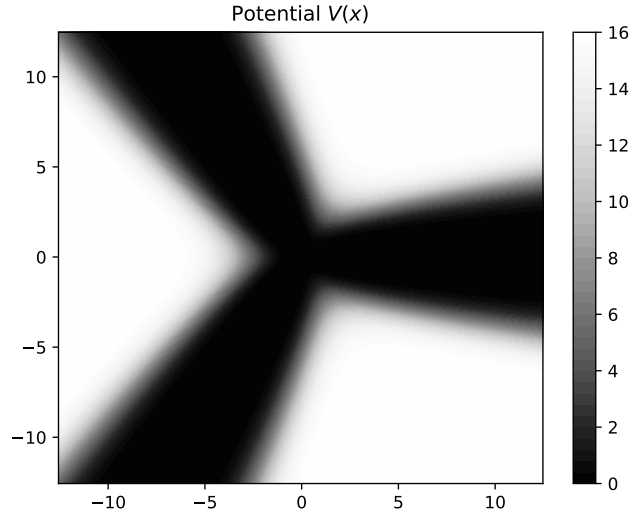


FIGURE 3.3. The threefold Morse potential. We expect a high probability of finding the particle within the back region, which is confirmed by Figure 3.5 below.

Finally, we take the Gaussian initial data

$$\psi_0(x) = \frac{1}{\sqrt{2\pi\sigma^2}} \exp\left(-\frac{(x-\mu)^2}{4\sigma^2} + 2ix_1\right), \quad \mu := \begin{pmatrix} 2 \\ 2 \end{pmatrix}, \quad \sigma^2 := \frac{1}{2}$$

of  $L^2$ -norm one. Write  $\psi(t) = \psi(x, t)$  and denote by  $\langle \cdot, \cdot \rangle_{L^2}$  the inner product on  $L^2(\mathbb{R}^d)$ . We consider the energies

$$\begin{aligned} E_{\text{kin}}(t) &:= \langle \psi(t), -\Delta \psi(t) \rangle_{L^2} && \text{(kinetic energy)} \\ E_{\text{mag}}(t) &:= \langle \psi(t), (H_{-B}(t) + \|B(t)x\|_{\mathbb{R}^d}^2) \psi(t) \rangle_{L^2} && \text{(magnetic energy)} \\ E_{\text{pot}}(t) &:= \langle \psi(t), \phi(x) \psi(t) \rangle_{L^2} && \text{(potential energy)} \\ E_{\text{tot}}(t) &:= E_{\text{kin}}(t) + E_{\text{mag}}(t) + E_{\text{pot}}(t). && \text{(total energy)} \end{aligned}$$

for  $d = 2$ . Figure 3.4 indicates that the total energy is preserved, although its components exhibit non-trivial behavior. Note also that  $H_{-B}(t)$  is not a positive semidefinite operator and hence the magnetic energy can be negative. Moreover, the  $L^2$ -norm is approximately constant as well. For the simulation, we use a dense Fourier grid of equidistant meshwidth  $8\pi \cdot 2^{-8}$  in each spacial direction filling the square  $[-4\pi, 4\pi]^2$ .

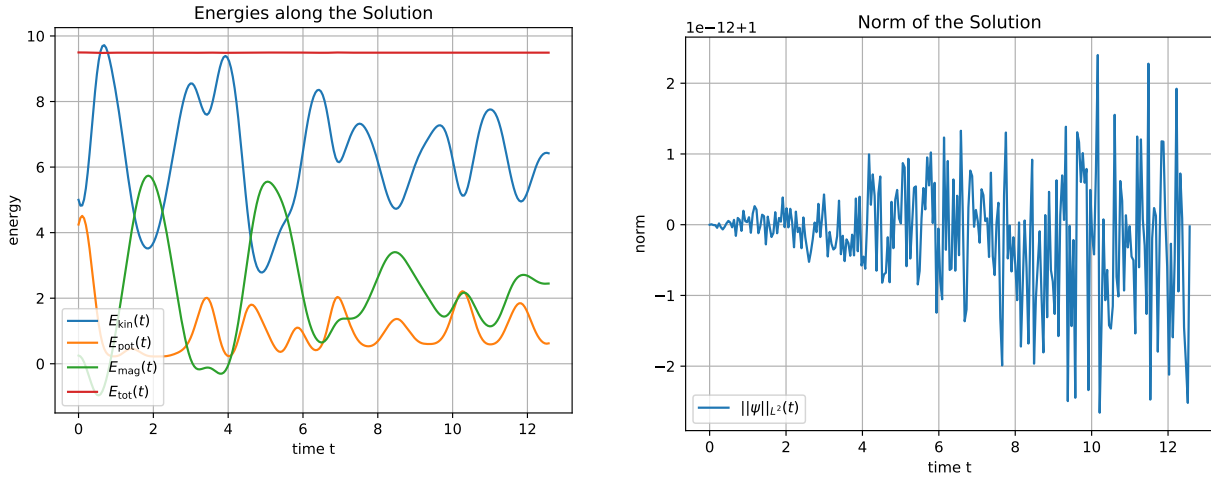


FIGURE 3.4. Energies and  $L^2$ -norm along the solution in the setting above. Note the scale on the right: The norm has oscillations of roughly  $10^{-12}$  around 1.

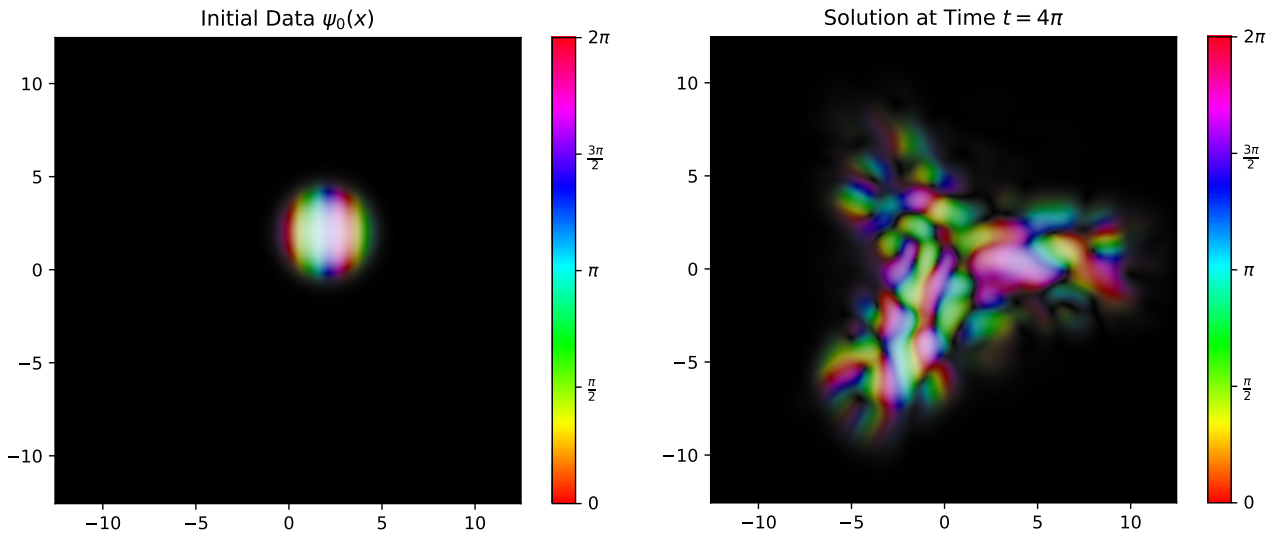


FIGURE 3.5. Initial data and solution in the setting above. A complex valued wave-function  $\varphi$  is plotted as follows: The color at  $x$  encodes the phase of  $\varphi(x)$ , while we darken the pixel according to the modulus  $|\varphi(x)|$ . A black pixel indicates a vanishing wave function at this point and the larger the value of  $|\varphi(x)|$ , the brighter the pixel at  $x$ .

### 3.5. Two Particles (Mie(4,2) Potential)

We consider two particles in two dimensions, i.e. Example 3.2 for  $N = 2$ . The initial data is given by

$$\psi_0(x^{(1)}, x^{(2)}) = \frac{1}{2\pi\sigma^2} \exp\left(-\frac{(x^{(1)} - \mu^{(1)})^2 + (x^{(2)} - \mu^{(2)})^2}{4\sigma^2} + 2ix_1^{(1)}\right),$$

where  $x^{(1)}, x^{(2)} \in \mathbb{R}^2$  correspond to the first and second particle, and

$$\mu^{(1)} := \begin{pmatrix} -2 \\ -1 \end{pmatrix}, \quad \mu^{(2)} := \begin{pmatrix} 1 \\ 1 \end{pmatrix}, \quad \sigma^2 := \frac{1}{2}.$$

We use the time-independent magnetic field

$$B(t) = \begin{pmatrix} 0 & -1 & 0 & 0 \\ 1 & 0 & 0 & 0 \\ 0 & 0 & 0 & -1 \\ 0 & 0 & 1 & 0 \end{pmatrix},$$

which corresponds to  $B_3(t) \equiv 1$  in Example 3.2. The electric potential is given by

$$\phi(x^{(1)}, x^{(2)}) = M_{0,1}(\|x^{(1)} - x^{(2)}\|_{\mathbb{R}^2}),$$

where for small  $\varepsilon \geq 0$ ,

$$M_\varepsilon(r) = 32 \left( \frac{3^4}{(r^4 + \varepsilon)} - \frac{3^2}{(r^2 + \varepsilon)} \right) + 8$$

approximates a repulsive Mie(4,2) potential [16]. We use  $\varepsilon = 0.1$  in the simulations below to avoid division by zero. See Figure 3.6 for plots of  $M_0(r)$  and  $M_{0.1}(r)$ . Because  $B(t)$  is constant in time, the total energy is conserved. Norm and energy of the solution to (H) in this setting are presented in Figure 3.7. Here, we use a dense Fourier grid of equidistant meshwidth  $8\pi \cdot 2^{-6}$  in each spacial direction filling the hypercube  $[-4\pi, 4\pi]^4$ .

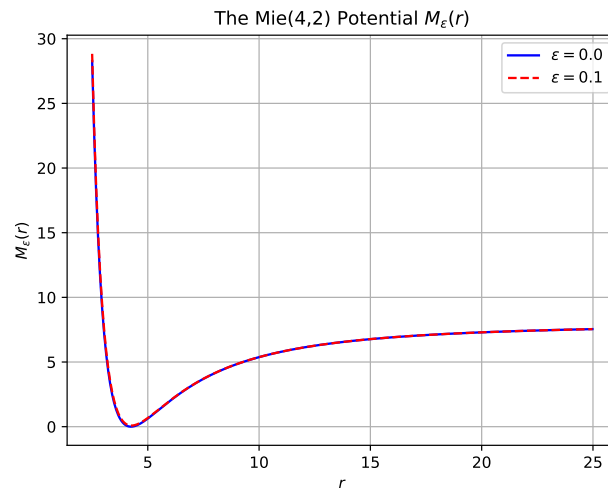


FIGURE 3.6. The potential  $M_\varepsilon(r)$ , where  $r > 0$  is the distance between the two particles.

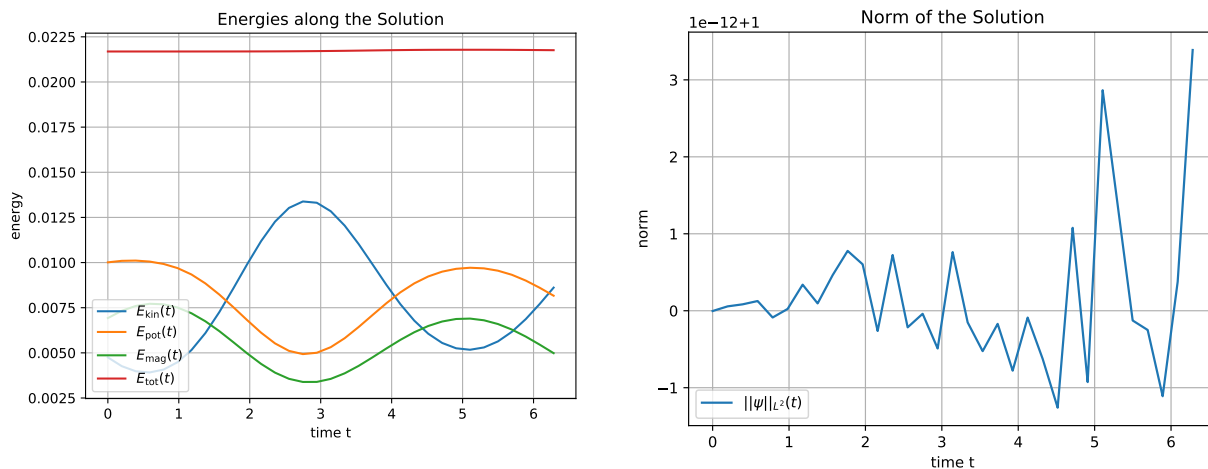


FIGURE 3.7. Energies and  $L^2$ -norm along the solution in the two-particle setting above. The separate energies are defined the same way as in Subsection 3.4. Note the scale on the right: The norm has oscillations of roughly  $10^{-12}$  around 1.

## References

- [1] S. Blanes and P. C. Moan. Splitting methods for the time-dependent Schrödinger equation. *Phys. Lett., A*, 265(1):35–42, 2000.
- [2] S. Blanes and P. C. Moan. Practical symplectic partitioned Runge–Kutta and Runge–Kutta–Nyström methods. *J. Comput. Appl. Math.*, 142(2):313–330, 2002.
- [3] S. Blanes and P. C. Moan. Fourth- and sixth-order commutator-free Magnus integrators for linear and non-linear dynamical systems. *Appl. Numer. Math.*, 56(12):1519–1537, 2006.
- [4] M. Caliari, A. Ostermann, and C. Piazzola. A splitting approach for the magnetic Schrödinger equation. *J. Comput. Appl. Math.*, 316:74–85, 2017. Selected Papers from NUMDIFF-14.
- [5] S. Descombes and M. Thalhammer. An exact local error representation of exponential operator splitting methods for evolutionary problems and applications to linear Schrödinger equations in the semi-classical regime. *BIT Numer. Math.*, 50(4):729–749, 2010.
- [6] S.-H. Dong. *Wave equations in higher dimensions*. Springer, 2011.
- [7] E. Faou, V. Gradinaru, and C. Lubich. Computing Semiclassical Quantum Dynamics with Hagedorn Wavepackets. *SIAM J. Sci. Comput.*, 31:3027–3041, 2009.
- [8] E. Hairer, S. P. Gheorghend Nørsett, and G. Wanner. *Solving Ordinary Differential Equations I (2nd Revised. Ed.): Nonstiff Problems*. Springer, 1993.
- [9] E. Hairer, C. Lubich, and G. Wanner. *Geometric numerical integration: Structure-preserving algorithms for ordinary differential equations*, volume 31 of *Springer Series in Computational Mathematics*. Springer, second edition, 2010.
- [10] B. C. Hall. *Quantum theory for mathematicians*, volume 267 of *Graduate Texts in Mathematics*. Springer, 2013.
- [11] S. Jin and Z. Zhou. A semi-Lagrangian time splitting method for the Schrödinger equation with vector potentials. *Commun. Inf. Syst.*, 13:247–289, 2013.
- [12] W. Kahan and R.-C. Li. Composition constants for raising the orders of unconventional schemes for ordinary differential equations. *Math. Comp.*, 66:1089–1099, 1997.

- [13] J. D. Louck. Generalized orbital angular momentum and the n-fold degenerate quantum-mechanical oscillator: Part II. The n-fold degenerate oscillator. *Journal of Molecular Spectroscopy*, 4(1):298–333, 1960.
- [14] Z. Ma, Y. Zhang, and Z. Zhou. An improved semi-Lagrangian time splitting spectral method for the semi-classical Schrödinger equation with vector potentials using NUFFT. *Appl. Numer. Math.*, 111:144–159, 2017.
- [15] W. Magnus. On the exponential solution of differential equations for a linear operator. *Commun. Pure Appl. Math.*, 7(4):649–673, 1954.
- [16] G. Mie. Zur kinetischen Theorie der einatomigen Körper. *Annalen der Physik*, 316(8):657–697, 1903.
- [17] W. Pauli. Zur Quantenmechanik des magnetischen Elektrons. *Zeitschrift für Physik*, 43(9):601–623, 1927.
- [18] B. Simon and M. Reed. *Fourier analysis, self-adjointness*, volume 2 of *Methods of modern mathematical physics*. Academic Press Inc., 1975.
- [19] G. Strang. On the construction and comparison of difference schemes. *SIAM J. Numer. Anal.*, 5:506–517, 1968.
- [20] G. Werth, V. N. Gheorghe, and F. G. Major. *Charged Particle Traps II: Applications*. Springer Series on Atomic, Optical, and Plasma Physics. Springer, 2009.
- [21] H. Yoshida. Construction of higher order symplectic integrators. *Phys. Lett., A*, 150(5):262–268, 1990.
- [22] Z. Zhou. Numerical approximation of the Schrödinger equation with the electromagnetic field by the Hagedorn wave packets. *J. Comput. Phys.*, 272:386–407, 2014.